**TITLE PAGE**

**Title:**

Trends of the anthropogenic $CO_2$ along 20ºW in the Iberian basin

**Authors:**

Fajar N. M., Pardo P. C., Carracedo L., Vázquez-Rodríguez M., Ríos A. F., Pérez, F. F.

**Address:**

Instituto de Investigacións Mariñas (CSIC). Eduardo Cabello 6, 36208 Vigo, Spain.

**Running title:**

Trends of the anthropogenic $CO_2$ in the Iberian basin

**Personal information**:

Noelia María Fajar González

Instituto de Investigacións Mariñas (CSIC). Eduardo Cabello 6, 36208 Vigo, Spain.

Tlf: 986 231 930 (Ext. 374)

E –mail: nfajar@iim.csic.es

**Abstract**

The carbon system in the water masses of the Iberian basin (North Atlantic Ocean) has been affected over the last two decades by the raise of the anthropogenic $CO_2$ ($C_{ant}$). In order to study the storage of $C_{ant}$ in the Iberian basin, the variables of the carbonic system were measured among others [i.e., pH, total inorganic carbon ($C_T$) and total alkalinity ($A_T$)] during the CAIBOX cruise. This cruise, conducted between July and August 2009 on board "B/O Sarmiento de Gamboa", was included on CAIBEX project (Shelf–ocean exchanges in the Canary–Iberian Large Marine Ecosystem). The storages of $C_{ant}$ were estimated using two different back-calculation techniques (i.e., $\varphi C_T^o$ method and TrOCA method) and for six layers of the water column corresponding to the approximate locations of the characteristic water masses of the region and layers of water masses mixing. For the whole water column and for the year 2009 the storages of $C_{ant}$ were of 88.1±3.8 and 93.7±3.7 $molC \cdot m^{-2}$ from $\varphi C_T^o$ and TrOCA methods, respectively. Moreover, the $C_{ant}$ storage rate from 1993 to 2009 was also estimated considering data from three additional cruises (OACES 1993, CHAOS 1998 and OACES 2003). The determined $C_{ant}$ storage rates were 1.41±0.25 and 1.67±0.13 $molC \cdot m^{-2} \cdot y^{-1}$ for $\varphi C_T^o$ and TrOCA methods, respectively. The increase of anthropogenic $CO_2$ uptake by the ocean can be seen when comparing these results with Ríos *et al.* (2001). Between the periods 1977-1997 and 1993-2009, the $C_{ant}$ concentration increased around 28-49 % in the first 2000m.

Key words: anthropogenic $CO_2$, back calculation

## 1. Introduction

Since the 18th century, the beginning of the industrial period, humankind has emitted large quantities of $CO_2$ into the atmosphere (Le Quéré 2009b) rising the global average atmospheric $CO_2$ from 280 ppm at the start of industrial revolution to 381 ppm in 2006 (Canadell *et al.* 2007). Nevertheless, less than a half of these emissions remain in the atmosphere and so, the anthropogenic $CO_2$ must have been taken up by the ocean or by the land biosphere (Sabine *et al.* 2004). Ongoing efforts are being taken to quantify the magnitude of these two sinks with high enough accuracy. Results from state-of-the-art models constrained the mean $CO_2$ uptake rates of land and ocean to 2.6±0.7 and 2.2±0.4 Pg C $y^{-1}$, respectively for the period 1990-2000. For the 2000-2008 period, the models estimated that the $CO_2$ uptake rates were 2.7±1.0 and 2.3±0.5 Pg C $y^{-1}$, for land and ocean respectively (Le Quéré *et al.* 2009a). These results show the variability of these $CO_2$ sinks and the decreasing trend in the ocean $CO_2$ uptake fraction. In fact, in spite of the increasing of the total amount of emitted $CO_2$, the oceanic $CO_2$ uptake fraction decreased from 27% in the period from 1990-2000 to 25% in 2000-2008 period. The main causes for this decrease could be a weak or limited transport rate of $CO_2$ from the surface to the deep ocean and also the nonlinearity in carbon chemistry that reduces the $CO_2$ capture capacity of water when its $CO_2$ concentration increases (Bindoff *et al.* 2007). As the World's Ocean reservoir accounts for approximately 90% of the natural carbon (Sabine & Tanhua 2010) a better knowledge of the variability in the rate of uptake and size of the ocean $CO_2$ sink is needed to predict global climate effects.

The attention of the marine scientific community is more concretely focussed on estimations of the anthropogenic component ($C_{ant}$) of the total inorganic carbon ($C_T$).

Despite all new techniques and technological progress, discerning between natural $CO_2$ and $C_{ant}$ is quite complex. In the end of XX century, back-calculation techniques have been developed to calculate $C_{ant}$ accumulation in the oceans (Brewer 1978). Back-calculation techniques were born with the aim of indirectly estimate $C_{ant}$ in the oceans by subtracting to $C_T$ the effects of remineralisation of organic matter (ROM), dissolution of calcium carbonate (Chen & Millero 1979) and $CO_2$ air-sea disequilibrium (Grubber *et al.* 1996). From them on, several kind of these methods have been applied to the global ocean or partial regions of it: ΔC* (Gruber *et al.* 1996), $C^o_{T_{IPSL}}$ (Lo Monaco *et al.* 2005), TrOCA (Körtzinger *et al.* 1998, Touratier *et al.* 2007) and $\varphi C^o_T$ (Pérez *et al.* 2008, Vázquez-Rodríguez *et al.* 2009a, hereinafter VR´09). Furthermore, other methods such as pCFC-age method ("shortcut method", Thomas & Ittekkot, 2001) and Transient Time Distribution (TTD) method (Waugh *et al.* 2006) emerged based on using CFCs as tracers to estimate the age for the water masses.

In this work, the Iberian basin, a specific region of the North Atlantic basin, was studied in terms of $C_{ant}$. The importance of the North Atlantic basin in terms of $C_{ant}$ storage stems from the fact that, despite covering only 15% of the global ocean area, the North Atlantic basin stores 23% of the total oceanic $C_{ant}$ (Sabine *et al.* 2004). The region of study is located in front of the Iberian peninsula and enclosed from 45ºN of latitude to the Canary Islands (25ºN) and between 20ºW and 8ºW of longitude (Fig. 1). This zone is inside the North Atlantic gyre, which is known as "the inter-gyre zone" (Pollard *et al.* 1996) enclosed between the North Atlantic Current (45-53ºN) and the Azores Current (34-35ºN, Péliz *et al.* 2005). The vertical thermohaline structure of this region (Carracedo *et al.* 2012 this issue) is clearly dominated in the upper layer by the Madeira Mode Water (MMW) (Álvarez *et al.*

2005), the East North Atlantic Central Water (ENACW) with differentiated branches of subpolar ($ENACW_P$) and subtropical ($ENACW_T$) origin (Ríos *et al.* 1992, Castro *et al.* 1998, Álvarez *et al.* 2005) and a little percentage of Antarctic Water (AA) (Ríos *et al.* 1992, Álvarez *et al.* 2005). Between intermediate and deep water masses it is important the presence of the Mediterranean Water (MW) (Fraga *et al.* 1982), which is the outflow from the Mediterranean Sea and the most saline water of the water column located at approximately 1000dbar. Deeper layers of the water column are dominated by the Labrador Sea Water (LSW) (Castro *et al.* 1998) while the North East Atlantic Deep Water (NEADW), divided in its upper ($NEADW_u$) and lower ($NEADW_l$) branches, and the Iceland Scotland Overflow Water (ISOW) are spanned in the bottom layers (Álvarez *et al.* 2005). The main properties of all these water masses are shown in Table 2.

Taking into account the thermohaline distribution in the Iberian basin and $A_T$, $C_T$, pH and nutrients measurements, estimations of $C_{ant}$ concentrations and $C_{ant}$ storage rates have been determined in the present work. Data collected during CAIBOX cruise in 2009 were used to estimate concentrations of $C_{ant}$. The estimated $C_{ant}$ was obtained through two different back-calculation techniques, $\varphi C_T^o$ and TrOCA, for 6 layers of the water column. In order to obtain the $C_{ant}$ storage rates, data from three earlier cruises (OACES 1993, CHAOS 1998, OACES 2003) were added closing almost two decadal periods. The $C_{ant}$ storages were compared between cruises and with the results that Pérez *et al.* (2010a) obtained for the Azores region. The estimated $C_{ant}$ storage rates were compared to the results of Ríos *et al.* (2001) obtaining considerable increments of the rates for the two back-calculating techniques applied. The higher increase of the oceanic $C_{ant}$ storage rate found for the last

111 decade in the Iberian basin can be a reflection of the corresponding increment reported for
112 the atmosphere.

113 ## 2. Data and methodology

114 The CAIBOX cruise was integrated in CAIBEX project ("Shelf-ocean Exchanges in
115 the Canary–Iberian Large Marine Ecosystem") and was spanned from 25th July to 14th
116 August in 2009 on board of B/O Sarmiento de Gamboa. This cruise was constituted by one
117 latitudinal section in front of Vigo coast (41.5ºN), one transversal section near the Canary
118 Islands (from 20ºW 30ºN to 13ºW 28.6ºN), and one longitudinal section along 20ºW (Fig
119 1). The longitudinal section was chosen for this study. A General Oceanic CTD with a 24
120 Niskin bottles (12 L) rosette was thrown in twenty four stations along the 20ºW section. In
121 each station 24 depth levels were selected depending on the bathymetry which varied from
122 3000m to more than 5000m. The distance between depth levels was approximately constant
123 in the first 1000m of the water column. Temperature, salinity, oxygen ($O_2$) and pH were
124 measured in each depth level, whereas nutrients and the rest of carbonic variables, i.e., pH,
125 total alkalinity ($A_T$), total inorganic carbon ($C_T$) were taken at specific depths according to
126 the thermohaline distribution.

127 The nutrients were determined by segmented flow analysis with a Technicon II
128 Autoanalyzer (Mouriño & Fraga 1985, Álvarez-Salgado *et al.*1992). The accuracy of nitrate
129 and phosphate was ±0.1 and ±0.01 $\mu mol \cdot kg^{-1}$, respectively. The $O_2$ samples were analysed
130 by the Winkler (1888) method.

131 Seawater pH measurements were made using the spectrophotometric method
132 described in Clayton & Byrne (1993) adding m-cresol purple as indicator. Absorbance
133 measurements were performed with a Shimadzu UV 2401. During all sessions the

134 temperature was controlled by a thermostatic bath at 25ºC. The precision of the
135 measurements with this method is estimated to be less than ±0.005 pH units (SOP 6b,
136 2007) and the values of pH are given in total scale.

137 Measurements of $A_T$ were done by a one endpoint method using an automatic
138 potentiometric titrator (Titrando 801 Metrohm) with a combined glass electrode (Mintrop *et*
139 *al.* 2000) obtaining a precision of less than ±2 $\mu mol \cdot kg^{-1}$ (SOP 3b 2008). Potentiometric
140 titration was carried out in an open flask (~250 $cm^3$) with HCl (0.1 M) and using two pH
141 endpoints very close between them, i.e., 4.45 and 4.42 (Pérez & Fraga 1987). In order to
142 estimate the accuracy of the $A_T$ method, alkalinity measurements of certified reference
143 material (CRM) of $CO_2$ from batch 84 provided by Dr. Andrew Dickson have been
144 analysed.

145 The $C_T$ was determined using a SOMMA (single-operator multiparameter metabolic
146 analyzers) system connected to a model CM101_093 coulometer (UIC.INC, Joliet,
147 ILLINOIS, USA, Johnson *et al.* 1998). The $CO_2$ is carried in this equipment by a free-$CO_2$
148 gas ($N_2$) into a coulometric cell, where it is quantitatively absorbed after reacting with
149 ethanolamine (Johnson *et al.* 1993). In every $C_T$-analysis session, calibrations were
150 performed with Certified Reference Material (CRM) of $CO_2$, supplied by Andrew Dickson
151 (Scripps Institution of Oceanography, University of California), to check for the accuracy
152 of the measurements. The precision of this method is ±4 $\mu mol \cdot kg^{-1}$ (SOP 2, 2007). In those
153 levels of the water column where $C_T$ data were not measured it was calculated from $A_T$ and
154 pH using the inorganic carbon system thermodynamic equations and the acid constants
155 from Mehrbach *et al.* (1973) fitted by Dickson & Millero (1987). The goodness of this

156 approximation can be seen in the Figure 2, where calculated $C_T$ fits well with measured $C_T$
157 ($R^2$=0.99).

158 Apart from CAIBOX cruise, other three cruises have been taken into account:
159 OACES 1993, CHAOS 1998 and OACES 2003 (Fig. 1, Table 1). Stations from each one of
160 them were selected in order to cover the area between 29ºN to 42ºN of latitude and 18ºW to
161 24ºW of longitude, near to the 20ºW longitudinal section of CAIBOX (Fig 1). The same
162 variables as in CAIBOX cruise were taken from the three additional cruises, which can be
163 downloaded from the CARINA website (Carbon in Atlantic Ocean;
164 http://cdiac.ornl.gov/oceans/CARINA/Carina_inv.html). With these additional data, the
165 combined dataset (20ºW CAIBOX cruise included) extends over 16 years (1993-2009).

166 Among all back-calculating techniques, two recent ones, TrOCA and $\varphi C_T^o$, have been
167 selected in order to obtain $C_{ant}$ estimations. Both of them are based on removing from $C_T$
168 the carbon contributions after the time of water mass formation due to oxidation/reduction
169 processes of organic matter and processes of dissolution of $CaCO_3$.

170 TrOCA method is an easy-to-apply technique because it only needs measurements of
171 potential temperature ($\theta$), $O_2$, $C_T$ and $A_T$ to define its TrOCA tracer (Tracer combinig
172 Oxygen, inorganic Carbon and total Alkalinity). The equation to obtain $C_{ant}$ is unique for
173 the whole ocean and the resulting estimations of $C_{ant}$ seem to be better correlated with
174 anthropogenic tracers (Touratier *et al.* 2007) than other methods as the classical $\Delta C^*$
175 (Gruber *et al.* 1996). The TrOCA approach estimates the anthropogenic $CO_2$ using the
176 following equation:

177 $$C_{ant}^{TrOCA} = \frac{TrOCA - TROCA^0}{a} \qquad (1)$$

178 where the tracer TrOCA is defined as:

179 $$\mathrm{TrOCA} = \mathrm{O_2} + \mathrm{a}\left(\mathrm{C_T} - \frac{1}{2}\mathrm{A_T}\right) \quad (2)$$

180 and $\mathrm{TrOCA^0}$ is a conservative tracer which was deduced from $\Delta^{14}C$ and CFC-11 tracers and
181 defined as:

182 $$\mathrm{TrOCA^0} = \mathrm{e}^{\left(\mathrm{b}+\mathrm{c}\cdot\theta+\frac{\mathrm{d}}{\mathrm{A_T^2}}\right)} \quad (3)$$

183 The dimensionless coefficients a, b, c and d on equations 1, 2 and 3 were properly
184 defined and established in Touratier *et al.* (2007) with an uncertainty associated to the $C_{ant}$
185 estimations of ±6.25 µmol·kg$^{-1}$.

186 On the other hand, the $\varphi C_T^o$ method is an approach oriented to biogeochemical
187 processes that introduces several improvements to the ΔC* method described by Lee *et al.*
188 (2003). This back-calculation method uses parameterizations of the terms of $A_T^0$ and $\Delta C_{dis}$
189 (i.e. preformed total alkalinity and air-sea disequilibrium of $CO_2$ at the moment of the water
190 mass formation) obtained from the sub-surface layer (100-200m), which accurately
191 represents the wintertime water masses formation conditions (VR'09). Apart from this
192 advantage, the $\varphi C_T^o$ method proposes an approximation to the horizontal (spatial) and
193 vertical (temporal) variability of $\Delta C_{dis}$ ($\Delta\Delta C_{dis}$) in terms of $C_{ant}$ and $\Delta C_{dis}$ itself. The $A_T^0$ and
194 $\Delta C_{dis}$ parameterizations are applied directly to calculate $C_{ant}$ in those waters above the 5ºC
195 isotherm. For cold deep waters (< 5ºC), the $\varphi C_T^o$ method improves the $C_{ant}$ estimations via
196 an extended Optimum MultiParameter (eOMP) analysis that take into account the water
197 masses mixing processes. The equation that describes $C_{ant}$ calculated from $\varphi C_T^o$ is the
198 following:

$$C_{ant} = \frac{\Delta C^{*} - \Delta C^{t}_{dis}}{1 + \varphi \frac{|\Delta C^{t}_{dis}|}{C^{sat}_{ant}}} \quad (4)$$

where $\Delta C^{t}_{dis}$ is the present-day $\Delta C_{dis}$, $C^{sat}_{ant}$ is the theoretical saturation concentration of $C_{ant}$ of the sample, depending mostly on the atmospheric *p*CO2 at the moment of the water mass formation, $\varphi = 0.55 \pm 0.10$ is a proportionality factor assumed to be constant elsewhere from the equator where it is positive, and $\Delta C^{*}$ is described after Gruber *et al* (1996):

$$\Delta C^{*} = C_T - \frac{AOU}{R_C} - 0.5(PA_T - PA^{0}_{T}) - C^{\pi}_{T,eq} \quad (5)$$

where $\frac{AOU}{R_C}$ and $0.5(PA_T - PA^{0}_{T})$ accounts for ROM and $CaCO_3$ dissolution, respectively, $AOU = O^{0}_{2,sat} - O_2$ is the Apparent Oxygen Utilization, $PA_T$ and $PA^{0}_{T}$ are the total and preformed potential alkalinity, respectively and $C^{\pi}_{T,eq}$ is the preformed total inorganic carbon concentration in equilibrium with the pre-industrial atmosphere.

Rigorous description of the $\varphi C^{o}_{T}$ method can be found in VR´09 who estimated an uncertainty of ±5.2 µmol·kg$^{-1}$ for the $C_{ant}$ estimation by a random propagation of the errors associated with the input variables. The MATLAB script to run $\varphi C^{o}_{T}$ method is available at the "$CO_2$ Group" webpage: http://oceano.iim.csic.es/co2group/index.html.

## 3. Results

$C_{ant}$ concentration (hereinafter [$C_{ant}$]) was estimated from $\varphi C^{o}_{T}$ and TrOCA methods for each of the cruises previously described, i.e., OACES 1993, CHAOS 1998, OACES 2003 and section 20ºW from CAIBOX 2009, and the distributions of the variable obtained with each method are shown in Figure 3. Negative values of [$C_{ant}$] using the TrOCA

219 method are showed as zeros in order to better visualize the differences. All plots show very
220 similar vertical gradients of [$C_{ant}$] independently of the methodology used in the
221 estimations, with the highest quantities in the warm surface waters and low values near the
222 bottom. The range of variation depends on the cruise (year) and slightly on the method and
223 gradually increases from 0-50 μmol·kg$^{-1}$ in OACES 1993 (Fig. 3a, b) to 0-70 μmol·kg$^{-1}$ in
224 CAIBOX 2009 (Fig. 3g, h). In general, $\varphi C_T^o$ method estimates [$C_{ant}$] slightly higher than
225 those from TrOCA method on deep waters (>3000dbar) for all the cruises. On the contrary,
226 [$C_{ant}$] estimated using TrOCA method are higher near the surface (<500dbar). In
227 intermediate layers both method estimate very similar [$C_{ant}$] values. Actually, both methods
228 show high determination coefficients on each cruise, as it can be seen in Figure 4.

229 In general, [$C_{ant}$] is importantly related to the characteristics of the water masses
230 present in the water column. The 20ºW section from CAIBOX cruise was selected in order
231 to study the distribution of the variables in the Iberian basin (Table 2, Fig. 5). AOU, $A_T$ and
232 $C_T$ distributions along the selected section are shown in Figure 5. The vertical thermohaline
233 structure is clearly dominated in the upper layers (<500dbar) by the NACW with values of
234 AOU ranging between 20-60 μmol·kg$^{-1}$ (Fig. 5a). At ~1000dbar in the south part of the
235 section, a little percentage of AA is identified by the AOU maximum (~110 μmol·kg$^{-1}$,
236 Fig.5a). At the same depth but in the centre of the section, MW emphasizes its presence
237 performing an $A_T$ maximum (2375 μmol·kg$^{-1}$, Fig.5b). In the north part of the section,
238 LSW shows its intense influence through AOU, $A_T$ and $C_T$ minima (Fig. 5a, b, c). The
239 distribution of $C_T$ (Fig. 5c) reveals the effect of biogeochemistry over the values of this
240 variable. In the upper layers (<500dbar) the lowest $C_T$ values (Fig. 5c) are due to the high
241 quantities of $CO_2$ taken up by the photosynthesis of primary producers. In deeper layers

(>3000dbar) the high values of $C_T$ (Fig. 5c) are due to the processes of ROM and $CaCO_3$ dissolution, which is also represented by the relatively high values of $A_T$ (Fig. 5b). The ROM is also detected by the steady and high values of AOU found at these depths (Fig. 5a).

In order to relate the values of $[C_{ant}]$ to the thermohaline distribution of the region, the water column was divided into six layers distinguished in base of density ranges. These density ranges were selected according to a T-S diagram performed with data from all the cruises (Fig. 6). The uppermost layers (NACW, MW, Fig. 6a) were delimited using 1000dbar as the pressure level of reference, while 2000dbar was the level of reference for deeper layers (Fig. 6b). NACW layer involves all data from surface to the isopycnal of 31.8 $kg \cdot m^{-3}$. MW layer contains all data from 31.8 to 32.25 $kg \cdot m^{-3}$ density isolines. Mixed MW-LSW layer includes all data between the 32.25 $kg \cdot m^{-3}$ isopycnal calculated at 1000dbar as level of reference and the 36.89 $kg \cdot m^{-3}$ isopycnal calculated at 2000dbar as level of reference. In deep waters, the LSW layer and the Deep Mixed layer can be distinguished enclosing all data between 36.89 and 36.95 $kg \cdot m^{-3}$, and 36.95 to 37.05 $kg \cdot m^{-3}$ isopycnals, respectively. At last, the upper and lower NEADW and the ISOW were included in the NADW (North Atlantic Deep Water) layer, which encloses data from the 37.05 $kg \cdot m^{-3}$ isopycnal to the bottom.

Once the layers have been defined, $[C_{ant}]$ values are obtained using $\varphi C_T^o$ and TrOCA methods and separately for each cruise (year). Mean $[C_{ant}]$ values are obtained for each layer through a vertical and horizontal integration (Pérez *et al.* 2010a). The thickness of each layer was computed as the average vertical distance between layers, weighted by the separation between stations. The vertical integration was done between the upper and lower

limits of the layers, while the limits in the horizontal integration were consequent with each cruise (Fig. 1). In Table 3, the average values of thickness and $[C_{ant}]$ estimated from $\varphi C_T^o$ ($[C_{ant}]_\varphi$) and TrOCA ($[C_{ant}]_{TrOCA}$) methods are shown for each layer and for each cruise (denoted by the year in which each one was performed). The integrated-average values of salinity, θ, and AOU are also shown. In general terms, the $[C_{ant}]$ tends to increase in all the layers and decreases downward in the water column, as was previously shown in Figure 3. The highest $[C_{ant}]_\varphi$ and $[C_{ant}]_{TrOCA}$ were found in the NACW layer for 2009 with values of 55.1±0.6 and 56.8±0.6μmol·kg$^{-1}$, respectively (Table 3). It must be emphasized the relatively high values of $[C_{ant}]_\varphi$ and $[C_{ant}]_{TrOCA}$ in the MW layer whose ranges vary from 18.8±0.9 to 28.9±0.7μmol·kg$^{-1}$ and 22.2±1.0 to 33.8±0.8 μmol·kg$^{-1}$, respectively (Table 3). $[C_{ant}]_\varphi$ and $[C_{ant}]_{TrOCA}$ are very similar for all layers and years being $[C_{ant}]_{TrOCA}$ slightly higher than $[C_{ant}]_\varphi$ in almost all the cases except for the NADW layer. The differences between $[C_{ant}]_\varphi$ and $[C_{ant}]_{TrOCA}$ range from 6.4 μmol·kg$^{-1}$ in the MW-LSW layer to 1.2 μmol·kg$^{-1}$ in the Deep Mixed layer (Table 3). In the NADW layer, $[C_{ant}]_\varphi$ shows values of around 3.0 μmol·kg$^{-1}$ higher than $[C_{ant}]_{TrOCA}$ (Table 3), being the average values of $[C_{ant}]_\varphi$ and $[C_{ant}]_{TrOCA}$ in this layer of 4.5±0.7 μmol·kg$^{-1}$ and 1.5±0.2 μmol·kg$^{-1}$, respectively. It is also noticeable in this deep layer that the variability of $[C_{ant}]_{TrOCA}$ between years is almost null compared to that of $[C_{ant}]_\varphi$. Furthermore, $C_{ant}$ storages are given for each year and each method estimated by the addition of $[C_{ant}]_\varphi$ and $[C_{ant}]_{TrOCA}$ in each layer multiplied by the thickness of the respective layer. The storages of $C_{ant}$ range between 66.9±4.1 molC·m$^{-2}$ and 88.1±3.8 molC·m$^{-2}$ for $\varphi C_T^o$ method and between 67.9±4.0 molC·m$^{-2}$ and 93.7±3.7 molC m$^{-2}$ for TrOCA method (Table 3). The storages obtained with TrOCA method are between 1 molC·m$^{-2}$ and 7 molC·m$^{-2}$ higher than those obtained with $\varphi C_T^o$ method for the

288 year 1993 and 2003, respectively. In general, the $C_{ant}$ storages increase with the year
289 independently of the method of estimation.

290 Despite the fact that a first overview of the temporal evolution of $[C_{ant}]$ between 1993
291 and 2009 can be perceived from previous results, temporal evolution of $[C_{ant}]_{\varphi}$ and
292 $[C_{ant}]_{TrOCA}$ for each layer together with that of $C_{ant}$ storages and $C_{ant}^{sat}$ (in $\mu mol \cdot kg^{-1}$) are
293 shown in Figure 7. In this figure, the decrease in $[C_{ant}]$ with depth and the generally higher
294 values of $[C_{ant}]_{TrOCA}$ (dashed lines in Fig. 7) respect to $[C_{ant}]_{\varphi}$ (solid lines in Fig. 7)
295 mentioned before can be also seen. It is also noticeable that storages estimated from
296 TrOCA method (iTrOCA, Fig. 7) are higher than those from $\varphi C_T^o$ method ($i\varphi C_T^o$, Fig. 7).
297 There is a general increasing trend in the $[C_{ant}]_{\varphi}$ and $[C_{ant}]_{TrOCA}$ in each of the layers and of
298 the $C_{ant}$ storages for both methods. The slopes of the different lines (Fig. 7) give the values
299 of $[C_{ant}]$ rates (in $\mu mol \cdot kg^{-1} \cdot y^{-1}$) and $C_{ant}$ storage rates (in $molC \cdot m^{-2} \cdot y^{-1}$) shown in Table 3.
300 The same pattern found for $[C_{ant}]$ is also seen in $[C_{ant}]$ rates with high values of the trend in
301 the upper layers and very low values in the NADW layer (Table 3). For instance, the $[C_{ant}]$
302 rate in the NACW layer varies from 0.85±0.24 to 0.95±0.13 $\mu mol \cdot kg^{-1}$ $y^{-1}$ estimated by
303 $\varphi C_T^o$ and TrOCA, respectively while in the NADW layer the $[C_{ant}]$ rates from $\varphi C_T^o$ and
304 TrOCA methods are of 0.01±0.07 and 0.02±0.01 $\mu mol \cdot kg^{-1} \cdot y^{-1}$, respectively (Table 3). It is
305 worth highlighting the high $[C_{ant}]$ rates that appear in the MW layer, i.e, 0.61±0.06 and
306 0.70±0.06 $\mu mol \cdot kg^{-1} \cdot y^{-1}$ for $\varphi C_T^o$ and TrOCA methods, respectively (Table 3). The $[C_{ant}]$
307 rates do not depend on neither of the two methods of estimation. Although $[C_{ant}]$ rates from
308 TrOCA method seem generally higher than those from $\varphi C_T^o$ method the differences
309 between them are not statistically significant. The trend for the $C_{ant}$ storage rates in the

studied region is also positive, with $C_{ant}$ storage rates of 1.41±0.25 and 1.67±0.13 molC·m$^{-2}$·y$^{-1}$ for $\varphi C_T^o$ and TrOCA, respectively.

## 4. Discussion

Two methods were used to estimate the distribution and temporal variability of [$C_{ant}$] along the Iberian Basin region, $\varphi C_T^o$ method and TrOCA method. Six vertical layers were defined in agreement with the thermohaline distribution of the region in order to relate the estimations of [$C_{ant}$] to the water masses present in the region. In general terms, the results obtained from both methods are quite similar, given the same pattern in the vertical distribution of [$C_{ant}$] (Fig. 3, Table 3). The values of [$C_{ant}$] are higher in the upper NACW layer (between 41.0±0.6 and 55.1±0.6 µmol·kg$^{-1}$ for $\varphi C_T^o$ method and between 42.0±0.6 and 56.6±0.6 µmol·kg$^{-1}$ for TrOCA method) but close to the expected values when seawater is in equilibrium with the increasing atmospheric $pCO_2$. These values progressively descend (Table 3, Fig. 7) from the upper layer to the NADW layer, where the [$C_{ant}$] are between 3.6±0.8 and 5.1±0.8 µmol·kg$^{-1}$ and between 1.4±0.8 and 1.7±0.7 µmol·kg$^{-1}$ for $\varphi C_T^o$ and TrOCA methods, respectively. Specifically, TrOCA method estimates higher values of [$C_{ant}$] than $\varphi C_T^o$ method for all layers except the NADW layer. This likely overestimation of [$C_{ant}$] by TrOCA method has been also concluded in the work of Yool *et al.* (2010), who analysed the method from a theoretical standpoint. The same results have been reported for the Atlantic basin after comparison with others back-calculation methods (Vázquez-Rodríguez *et al.* 2009b). Moreover, Huertas *et al.* (2009) found an increase of [$C_{ant}$] estimated by TrOCA method with depth in the Gibraltar Strait, contrary to the results present here, which points out the not-universal appliance of TrOCA method. Even in a

completely different oceanic area, the eastern South American coast (Ríos *et al.* 2010) high values of $[C_{ant}]_{TrOCA}$ (some of them over the theoretical limit of $C_{ant}^{sat}$) have been found in the upper layers. The reason for this bias in TrOCA method probably relays on the assumption that air-sea flux of $CO_2$ scales with temperature and alkalinity (Yool *et al.* 2010). In the NADW layer the estimations of $[C_{ant}]_{TrOCA}$ are lower than $[C_{ant}]_{\varphi}$. Actually, the low values of $[C_{ant}]_{TrOCA}$ for this layer are obtained after assuming zero all negative $[C_{ant}]_{TrOCA}$ estimations (approximately 70% of TrOCA estimations in the NADW layer are negative), which help in terms of comparison between methods but corroborates the existence of important bias in TrOCA method at least in some areas. Negative results around bottom layers using TrOCA method were also observed for the whole Atlantic Ocean by Vázquez-Rodríguez *et al.* (2009b). On the other hand, $[C_{ant}]_{\varphi}$ never exceed the $C_{ant}^{sat}$ values in the upper layers because the $\varphi C_T^o$ method is limited in surface to saturation values and it is constrained to keep negative disequilibria ($\Delta\Delta C_{dis}<0$) in relation to the pre-industrial era (VR'09). These slight differences between both methods estimations can also be a consequence of the $\Delta\Delta C_{dis}$ term. This term is assumed zero in the TrOCA method whereas in the $\varphi C_T^o$ method it stems from the main assumption that $\Delta C_{dis}$ vary with time, contrary to the classical assumption of invariability of $\Delta C_{dis}$ in the classical back-calculating methods (Gruber *et al.* 1996, Lo Monaco *et al.* 2005, Sabine & Tanhua 2010). This same pattern, i.e., higher values of $[C_{ant}]_{TrOCA}$ in all water column except near the bottom where $[C_{ant}]_{\varphi}$ are higher than $[C_{ant}]_{TrOCA}$ estimations, is also found in the Azores region (Pérez *et al.* 2010a), which is a very close region to the Iberian basin.

The $C_{ant}$ storages obtained separately for each cruise were also very similar for both methods varying from 66.9±4.1 to 88.1±3.8 molC·m$^{-2}$ for $\varphi C_T^o$ method and from 67.9±4.0

to 93.7±3.7 molC·m$^{-2}$ for TrOCA method and clearly indicating an increase of the $C_{ant}$ storage of the Iberian basin with time. In order to have a quantitative comparison of these data, results from the work of Pérez *et al.* (2010a) in the Azores region were considered. In this work, data from the AZORES I (1998), OACES 1993 and METEOR 2004 cruises were studied among others. OACES 1993 is also included in this work and the other two cruises are inside the period of time studied here. Pérez *et al*. (2010a) obtained higher values of the $C_{ant}$ storages in the OACES 1993, with differences respect to the results obtained here of ~3 molC·m$^{-2}$ and ~6 molC·m$^{-2}$ for $\varphi C_T^o$ and TrOCA method, respectively. Interestingly, these differences are attributed to the different methodology in the vertical integration of [$C_{ant}$] which in Pérez *et al.* (2010a) was made in base of an average profile of [$C_{ant}$] and not in base of a more-realistic mean-layered [$C_{ant}$] as it was done here. Moreover, for the Iberian basin more stations than in Pérez *et al.* (2010a) were taken into account. The $C_{ant}$ storage estimated for AZORES I (Pérez *et al.* 2010a) was ~10 molC·m$^{-2}$ (approximated for the two back-calculating methods) higher than the value found here for CHAOS 1998. In spite of the different vertical integration method, this difference could also be due to the different location of AZORES I cruise (Fig. 1 in Pérez *et al.* 2010a) respect to CHAOS 1998 (Fig. 1). AZORES I spans close to the Mid-Atlantic Ridge, so higher proportions of LSW with high [$C_{ant}$] are sampled. Nonetheless, the METEOR 2004 cruise gives $C_{ant}$ storages of 87±1 and 92±1 molC·m$^{-2}$ for $\varphi C_T^o$ and TrOCA, respectively (Pérez *et al.* 2010a), very close to those values for OACES 2003 (78.9±4.2 and 85.0±4.1 molC·m$^{-2}$ for $\varphi C_T^o$ and TrOCA, respectively) but higher, thus corroborating the temporal increase in the $C_{ant}$ storage of the Iberian basin. In this sense, there is also good consistence with the $C_{ant}$ storages of 87±5

and 95±5 molC·m$^{-2}$ for $\varphi C_T^o$ and TrOCA methods, respectively, obtained for the Biscay Bay during VACLAN-2005 (Castaño-Carrera *et al.* 2012, in this issue).

The [$C_{ant}$] rates estimated in the Iberian basin for each one of the layers show high values in the NACW layer and in the MW layer (~0.90 and ~0.65 µmol·kg$^{-1}$·y$^{-1}$, respectively) and a progressive descend of the rates toward the bottom. For the whole water column, the $C_{ant}$ storage rates were 1.41±0.25 molC·m$^{-2}$·y$^{-1}$ for $\varphi C_T^o$ method and 1.67±0.13 molC·m$^{-2}$·y$^{-1}$ for TrOCA method. Importantly, all rates show no-statistically significant differences between the two estimating methods. No methodology dependent results were also obtained by Pérez *et al.* (2010a) for the period 1981-2004 in the Azores region, where the $C_{ant}$ storage rates were 1.32±0.11 molC·m$^{-2}$·y$^{-1}$ for $\varphi C_T^o$ method and 1.18±0.16 molC·m$^{-2}$·y$^{-1}$ for TrOCA method. The $C_{ant}$ storage rates found here for the period 1993-2009 are higher than those found by Pérez *et al.* (2010a) which can be a signal of an acceleration of the $C_{ant}$ uptake by the ocean, at least in the Iberian basin region.

In order to look for a more reliable sign of this acceleration $C_{ant}$ storage rate estimations from older periods of time can be of great help. From 1977 to 1997, Ríos *et al.* (2001) estimated [$C_{ant}$] in the Iberian Peninsula coast by a back-calculation technique obtaining a $C_{ant}$ storage rate of 0.95 molC·m$^{-2}$·y$^{-1}$ for the upper 2000m. In order to compare two periods of time, all data (1993-2009) were recalculated for the first 2000m in the Iberian basin, finding that the average percentage of $C_{ant}$ storage between 0-2000m represents 80.6±1.4 and 86.7±1.1 % of the total $C_{ant}$ storage for $\varphi C_T^o$ and TrOCA, respectively. Thus, the $C_{ant}$ storage rates in the upper 2000m estimated by $\varphi C_T^o$ and TrOCA method are 1.21±0.18 and 1.42±0.19 molC·m$^{-2}$·y$^{-1}$, respectively. These rates, respect to the

value found by Ríos *et al.* (2001), mean an increase of $C_{ant}$ storage rate of around 28% considering $\varphi C_T^o$ method and of ~49% according to TrOCA method.

The cause of this increase in the $C_{ant}$ storage rate found in the Iberian basin could be linked to a similar increase in the atmospheric $CO_2$. According to the Mauna Loa annual mean $CO_2$ data (Dr Pieter Tans, NOAA/ESRL http:/www.esrl.noaa.gov/gmd/ccgg/trends) the atmospheric $CO_2$ increased from ~334 ppm in 1977 to ~387 ppm in 2009. Splitting these increasing trends into the two periods previously mentioned, 1977-1997 and 1993-2009, the average $CO_2$ rates were 1.49±0.02 and 1.92±0.02 $ppm \cdot y^{-1}$, for each period respectively. The increase of $CO_2$ rate in the atmosphere is of ~29%, which is a value very close to the increase in the ocean $C_{ant}$ storage rate found here (~28-49%). Nevertheless, Pérez *et al.* (2010b), for the region of the North Atlantic Subpolar Gyre (where the Iberian basin region is partially included) found a decrease of ~48% in the $C_{ant}$ storage rates from the first half of the 1990s to the period 1997-2006. According to Pérez *et al.* (2010b) this decrease is linked to the high and low NAO phases which act over the volumetric census of the water masses present in the region. As can be deduced from these results, the storage rates can vary between close areas depending on the dynamics of the region and also on the time period studied. Owing to all these different quantities found, more insight into $C_{ant}$ storages and $C_{ant}$ storages rates is needed in order to get a better understanding of the carbon cycle in the atmosphere-ocean system.

**Acknowledgements**

The authors thank the cruise participants, both the B/O Sarmiento de Gamboa crew and the scientific and technical team, for their indispensable help. We are also very grateful to X. A. Álvarez-Salgado and V. Viéitez dos Santos for providing us the nutrient data.

Part of the data presented in this paper has been obtained by means of CAIBEX Project: *Shelf-ocean exchanges in the Canary-Iberia Large Marine Ecosystem* (CTM2007-66408-C02/MAR), supported by the Spanish Council of Education and Science.

The first author is funded by a predoctoral fellowship of the program JAE "Junta para la Ampliación de Estudios" from the Consejo Superior de Investigaciones Científicas (CSIC).

## References

Álvarez-Salgado X. A., Fraga F., Pérez F. F., 1992. Determination of nutrient salts both in sea and brackish waters by automatic methods. The phosphate blank. Marine Chemistry 39: 311–319.

Álvarez M., Pérez F. F., Shoosmith D.R., Bryden H. L., 2005. Unaccounted role of Mediterranean Water in the drawdown of anthropogenic carbon. J. Geophys. Res., 110, C09S03, doi:10.1029/2004JC002633.

Bindoff, N. L., J. Willebrand, V. Artale, A, Cazenave, J. Gregory, S. Gulev, K. Hanawa, C. Le Quéré, S. Levitus, Y. Nojiri, C.K. Shum, L.D.Talley and A. Unnikrishnan, 2007: Observations: Oceanic Climate Change and Sea Level. In: Climate Change 2007: The Physical Science Basis. Contribution of Working Group I to the Fourth Assessment Report of the Intergovernmental Panel on Climate Change [Solomon, S.,D. Qin, M. Manning, Z. Chen, M. Marquis, K.B. Averyt, M. Tignor and H.L. Miller (eds.)]. Cambridge University Press, Cambridge, United Kingdom and New York, NY, USA.

Brewer P.G., 1978. Direct observation of the oceanic $CO_2$ increase. Geophys. Res. Lett. 5 997-1000.

Canadell J., C. Le Quéré, M. R. Raupach, C. Fields, E.T. Buitenhuis, P. Ciais, T. J. Conway, N.P. Gillett, R. A. Houghton and G. Marland., 2007. Contributions to accelerating atmospheric $CO_2$ growth from economic activity, carbon intensity, and efficiency of natural sinks. Proc. Natl. Acad. Sci. U. S. A., doi:10.1073/pnas.0702737104.

Carracedo L. I.; Pardo P. C.; Villacieros-Robineau N.; De la Granda F.; Gilcoto M.; Pérez F. F., 2010. Temporal changes of the water masses distribution and transports along the 20ºW CAIBOX section (NE Atlantic). Ciencias Marinas (this issue).

Castaño-Carrera M., Pardo P. C., Álvarez M., Lavín A., Rodríguez C., Ríos A. F., Carballo R., González N., Pérez F. F., 2010. Anthropogenic carbon and water masses in the Bay of Biscay. Ciencias Marinas (this issue).

Castro C.G., Pérez F. F., Holley S. E., Rios. A.F., 1998. Chemical characterisation and modelling of water masses in the Northeast Atlantic. Prog. Oceanog. 41 (3): 249-279.

Chen C. T., Millero, F. J., 1979. Gradual increase of oceanic carbon dioxide. Nature 277 205–206.

Clayton T., Byrne. R. H., 1993. Spectrophotometric seawater pH measurements: Total hydrogen ion concentration scale concentration scale calibration of m-cresol purple and at-sea results. Deep Sea Res. (Part I) 40: 2115–2129.

Dickson A.G., Millero F.J., 1987. A comparison of the equilibrium constants for the dissociation of carbonic acid in seawater media. Deep-Sea Research I 34: 1733–1743.

Fraga F., Mouriño C., Manriquez M., 1982. Las masas de agua en la costa de Galicia: junio-octubre. Res. Exp. Cient. 10 51-77.

Gruber N., Sarmiento J. L., Stocker T. F., 1996. An improved method for detecting anthropogenic $CO_2$ in the oceans. Global Biogeochem. Cycles 10(4): 809–837 doi:10.1029/96GB01608.

Huertas I. E., Ríos A. F., García-Lafuente J., Makaoui A., Rodríguez-Gálvez S., Sánchez-Román A., Orbi A., Ruíz J., Pérez F. F., 2009. Anthropogenic and natural $CO_2$ exchange through the Strait of Gibraltar. Biogeoscience 6: 647-662

Johnson K. M., Wills K. D., Butler D. B., Johnson W. K., Wong. C. S., 1993. Coulometric total carbon dioxide analysis for marine studies: maximizing the performance of an automated gas extraction system and coulometric detector. Marine Chemistry 17: 1–21.

Johnson K.M., Dickson A. G., Eischeid G., Goyet C., Guenther P., Key R. M., Millero F. J., Purkerson D., Sabine C. L., Schottle R. G., Wallace D.W.R., Wilke R. J., Winn C. D., 1998. Coulometric total carbon dioxide analysis for marine studies: assessment of the quality of total inorganic carbon measurements made during the US Indian Ocean CO Survey 1994–1996. Marine Chemistry 63: 21–37.

Körtzinger A., Mintrop, L., Duinker, J. C., 1998. On the penetration of anthropogenic $CO_2$ into the North Atlantic Ocean. J. Geophys. Res. 103: 18,681–18,689

Le Quéré C., Raupach M. R., Canadell J. G., Marland G., Bopp L., Ciais P., Conway T. J., Doney S. C., Feely R. A., Foster P., Friedlingstein P., Gurney K., Houghton R. A., House J. I., Huntingford C., Levy P. E., Lomas M. R., Majkut J., Metzl N., Ometto J. P., Peters G. P., Prentice I. C., Randerson J. T., Running S. W., Sarmiento J. L., Schuster U., Sitch S.,Takahashi T., Viovy N., van der Werf G. R.,Woodward F. I., 2009a. Trends in the sources and sinks of carbon dioxide. Nature Geoscience 2: 831-836.

Le Quéré 2009b. Closing the glogal budget for $CO_2$. Global Change 74: 28-31.

Lee K., Choi, S.-D. Park, G.-H. Wanninkhof, R., 2003. An updated anthropogenic $CO_2$ inventory in the Atlantic Ocean. Global Biogeochemical Cycles 17 (4): 1116-1133 doi: 10.1029/2003GB002067.

Lo Monaco C., Metzl N., Poisson A., Brunet C., Schauer B., 2005. Anthropogenic $CO_2$ in the Southern Ocean : distribution and inventory at the Indo-Atlantic boundary (WOCE line I6), J. Geophys. Res. 110, C06010, doi:10.1029/2004JC002643.

Mehrbach C., Culberson C. H., Hawley J. E., Pytkowicz R. M., 1973. Measurement of the apparent dissociation constants of carbonic acid in seawater at atmospheric pressure. Limnol. Oceanog. 18: 897–907.

Mintrop L., Pérez F. F., González-Davila M., Santana-Casiano M. J., Kortzinger, A., 2000. Alkalinity determination by potentiometry: Intercalibration using three different methods. Ciencias Marinas 26 (1): 23-37.

Mouriño C., Fraga, F., 1985. Determinacion de nitratos en agua de mar. Investigación Pesquera 49: 81–96.

Péliz A, Dubert J, Santos AMP, Oliveira PB, LeCann B. 2005. Winter upper ocean circulation in the western Iberian basin, fronts, eddies and poleward flows: an overview. Deep-Sea Research I. 52(4): 621-646.

Pérez F. F., Fraga, F., 1987. A precise and rapid analytical procedure for alkalinity determination. Mar. Chem. 21: 169–182.

Pérez F. F., Vázquez-Rodríguez, M., Louarn, E., Padín, X. A., Mercier, H., Ríos, A. F., 2008. Temporal variability of the anthropogenic $CO_2$ storage in the Irminger Sea. Biogeosciences 5: 1669–1679.

Pérez F. F., Arístegui J., Vázquez-Rodríguez M., Ríos A. F., 2010a. Anthropogenic $CO_2$ in the Azores region. Sciencia Marina 74S1 11-19doi:10.3989.

Pérez F. F., Vázquez-Rodríguez, M., Mercier, H., Velo, A., Ríos, A. F., 2010b. Trends of anthropogenic $CO_2$ storage in North Atlantic water mass. Biogeosciences 7: 1–19.

Pollard R. T., Griffiths M. J.,Cunninghan S. A., Read J. F., Pérez F. F., Ríos A. F., 1996. Vivaldi 1991- A study of the formation, circulation and ventilation of Eastern North Atlantic Central Water. Progress Oceanography 37: 167-192

Ríos A. F., Pérez F. F., Fraga F., 1992. Water masses in the upper and middle North Atlantic Ocean east of the Azores. Deep-Sea Research 39: 645-658.

Ríos A. F., Pérez F. F., Fraga F., 2001. Long-term (1977-1997) measurements of carbon dioxide in the Eastern North Atlantic: evaluation of anthropogenic input. Deep-Sea Research II 48: 2227-2239.

Ríos A. F., Vázquez-Rodríguez M., Padín X. A., Pérez F. F., 2010. Anthropogenic carbon dioxide in the South Atlantic western basin. Journal of Marine Systems 83: 38–44.

Sabine C. L., Feely R. A., Gruber N., Key R. M., Lee K., Bullister J. L., Wanninkhof R., Wong C. S., Wallace D. W. R., Tilbrook B., Millero F. J.,Peng T.-H., Kozyr A., Ono T., Rios A. F., 2004. The Oceanic Sink for Anthropogenic $CO_2$. Science 305: 367-371.

Sabine C. L., Tanhua T., 2010. Estimation of Anthropogenic $CO_2$ Inventories in the Ocean. Annu. Rev. Marine. Sci. 2: 175-198.

SOP 2 (2007), SOP 3b (2008) and SOP 6b (2007) inside Dickson A.G., Sabine C.L., Christian J.R., 2007. Guide to best practices for ocean CO2 measurements. PICES Special Publication 3, 191 pp.

Thomas H., Ittekkot V., 2001. Determination of anthropogenic $CO_2$ in the North Atlantic Ocean using water mass ages and $CO_2$ equilibrium chemistry. Journal Marine Systems 27: 325-336.

Touratier F., Azouzi L., and Goyet C., 2007. CFC-11, $\Delta^{14}C$ and $^{3}H$ tracers as a means to assess anthropogenic $CO_2$ concentrations in the ocean. Tellus B 59B: 318–325 doi:10.1111/j.1600- 0889.2006.00247.x.

Vázquez-Rodríguez M., Padín X. A., Ríos A. F., Bellerby R. G. J., Pérez F. F., 2009a. An upgraded carbon-based method to estimate the anthropogenic fraction of dissolved $CO_2$ in the Atlantic Ocean. Biogeosciences Discuss. 6: 4527-4571 doi:10.5194/bgd-6-4527-2009 (http://www.biogeosciences-discuss.net/6/4527/2009/bgd-6-4527-2009.html)

Vázquez-Rodríguez M., Touratier F., Lo Monaco C., Waugh D. W., Padín X. A., Bellerby R. G. J, Goyet C., Metzl N., Ríos A. F., Pérez F. F., 2009b. Anthropogenic carbon distributions in the Atlantic Ocean: data-based estimates from the Arctic to the Antarctic. Biogeosciences 6: 439-451 doi:10.5194/bg-6-439-2009 (http://www.biogeosciences.net/6/439/2009/bg-6-439-2009.html)

Waugh D. W., Hall T. M., McNeil B. I., Key R., Matear R., 2006. Anthropogenic $CO_2$ in the oceans estimated using transit time distributions. Tellus B, 58: 376-389.

557 Winkler L. W. 1888. Die Bestimmung des im Wasser gelösten Sauerstoffes. Berichte
558 der deutschen chemischen Gesellschaft, 21: 2843–2854. doi:10.1002/cber.188802102122.

559 Yool A., Oschlies A., Nurser A. J. G., Gruber N., 2010. A model-based assessment of
560 the TrOCA approach for estimating anthropogenic carbon in the ocean. Biogeoscience 7:
561 723-751.

562

563 **Tables and table captions**

564

565 Table 1. Summary of the characteristics of the cruises taken into account for the
566 study. The year, the principal investigator (P.I.) and the number of stations are shown for
567 each cruise .

568

| ***CRUISE INFORMATION*** | | | | | |
|---|---|---|---|---|---|
| *Cruise* | *Section* | ***Year*** | ***P.I.*** | ***Expocode*** | ***Stations*** |
| OACES 1993 | OACES/$CO_2$-93 | 1993 | R. Wanninkhof | OACES93_A16N | 83 |
| CHAOS 1998 | WOCE A16N/AR21 | 1998 | Smythe-Wright | 74DI19980423 | 137 |
| OACES 2003 | CLIVAR A16N | 2003 | J. Bullister, N. Gruber | 3RO20030604 | 150 |
| CAIBOX 2009 | CAIBOX | 2009 | E. D. Barton | CAIBOX09 | 73 |

569

570

571

572

573

574

575

576

577 Table 2. Characteristic properties (θ, salinity, nutrients, $A_T$, $C_T$ and $O_2$) of the main
578 water masses present in the Iberian basin region: Antartic Water (AA), Subpolar East North
579 Atlantic Central Water ($ENACW_P$), Subtropical East North Atlantic Central Water
580 ($ENACW_T$), Iceland Scotland Overflow Water (ISOW), Labrador Sea Water (LSW),
581 Madeira Mode Water (MMW), Mediterranean Water (MW), Lower North East Atlantic
582 Deep Water ($NEADW_l$) and Upper North East Atlantic Deep Water ($NEADW_u$).

583

| Water mass | θ, °C | Salinity, psu | $SiO_4$, mmol | $NO_3$, mmol | $PO_4$, mmol | $A_T$, mmol | $O_2$, mmol | $C_T$, mmol |
|---|---|---|---|---|---|---|---|---|
| $ENACW_T$ | 15.3±0.4 | 36.1±0.02 | 2.24±1.7 | 2.12±1.2 | 0.15±0.05 | 2363±10 | 244±3 | 2096±6 |
| $ENACW_P$ | 8.3±0.3 | 35.23±0.01 | 10.33±0.6 | 9.58±1.3 | 0.73±0.08 | 2320±7 | 285±2 | 2112±12 |
| MW | 11.74±0.1 | 36.5±0.01 | 8.62±0.8 | 5.16±0.8 | 0.31±0.1 | 2411±1 | 262±5 | 2151±4 |
| LSW | 3.4±0.2 | 34.89±0.12 | 9.85±2.5 | 12.03±0.7 | 0.91±0.02 | 2301±7 | 320±2 | 2118±19 |
| ISOW | 1.93±0.08 | 34.96±0.02 | 11.12±5 | 9.26±2.7 | 0.85±0.13 | 2290±3 | 331±3 | 2099±4 |
| $NEADW_u$ | 2.4±0.003 | 34.93±0.003 | 35±6 | 11.95±0.2 | 0.9±0.07 | 2359±2 | 328±2 | 2139±22 |
| $NEADW_l$ | 1.92±0.003 | 34.88±0.002 | 49.85±5 | 12.94±0.4 | 1.02±0.03 | 2360±2 | 332±3 | 2147±10 |
| AA | 7.5±0.1 | 35±0.02 | 24.9±0.8 | 12.4±3.3 | 0.96±0.3 | 2320±1 | 290±2 | 2092±4 |
| MMW | 20±0.5 | 37±0.04 | 0.39±0.3 | 0.23±0.01 | 0.01±0.06 | 2418±13 | 223±9 | 2103±3 |

584
585

586

587 Table 3. Mean values (± standar error of the estimation) of thickness, salinity (Sal),
588 potential temperature (θ), apparent oxygen utilization (AOU) and [$C_{ant}$] estimated from
589 $\varphi C_T^o$ and TrOCA methods in each one of the six layers defined. $C_{ant}$ storages for each year
590 are also shown together with the [$C_{ant}$] rates for each layer and the $C_{ant}$ storage rates for the
591 water column.

592

| Year | Thickness (m) | Salinity | θ (ºC) | AOU (µmol kg$^{-1}$) | $[C_{ant}]_{\varphi}$ (µmol kg$^{-1}$) | $[C_{ant}]_{TrOCA}$ (µmol kg$^{-1}$) | $[C_{ant}]_{\varphi}$ rate (µmol kg$^{-1}$y$^{-1}$) | $[C_{ant}]_{TrOCA}$ rate (µmol kg$^{-1}$y$^{-1}$) |
|---|---|---|---|---|---|---|---|---|
| NACW | | | | | | | 0.85 ± 0.24 | 0.95 ± 0.13 |
| 1993 | 753 ± 11 | 35.947 ± 0.001 | 13.979 ± 0.002 | 45.7 ± 0.1 | 41.0 ± 0.6 | 42.0 ± 0.6 | | |
| 1998 | 729 ± 21 | 35.876 ± 0.001 | 13.467 ± 0.002 | 44.9 ± 0.1 | 42.9 ± 0.6 | 43.9 ± 0.6 | | |
| 2003 | 736 ± 25 | 35.926 ± 0.001 | 14.341 ± 0.002 | 42.1 ± 0.1 | 45.0 ± 0.5 | 50.7 ± 0.5 | | |
| 2009 | 722 ± 11 | 35.878 ± 0.001 | 13.652 ± 0.002 | 42.9 ± 0.1 | 55.1 ± 0.6 | 56.6 ± 0.6 | | |
| MW | | | | | | | 0.61 ± 0.06 | 0.70 ± 0.06 |
| 1993 | 481 ± 31 | 35.492 ± 0.001 | 8.443 ± 0.004 | 104.6 ± 0.2 | 18.8 ± 1.1 | 22.2 ± 0.9 | | |
| 1998 | 545 ± 39 | 35.556 ± 0.001 | 8.857 ± 0.004 | 100.4 ± 0.2 | 21.9 ± 1.0 | 25.8 ± 1.0 | | |
| 2003 | 473 ± 32 | 35.565 ± 0.001 | 8.913 ± 0.003 | 99.2 ± 0.1 | 23.9 ± 0.7 | 28.2 ± 0.7 | | |
| 2009 | 509 ± 15 | 35.653 ± 0.001 | 9.148 ± 0.003 | 94.2 ± 0.1 | 28.9 ± 0.6 | 33.8 ± 0.8 | | |
| MW-LSW | | | | | | | 0.32 ± 0.07 | 0.40 ± 0.06 |
| 1993 | 446 ± 48 | 35.305 ± 0.001 | 5.891 ± 0.004 | 76.0 ± 0.2 | 15.9 ± 1.0 | 21.6 ± 0.9 | | |
| 1998 | 420 ± 47 | 35.273 ± 0.001 | 5.689 ± 0.004 | 72.5 ± 0.2 | 16.0 ± 1.3 | 22.3 ± 1.4 | | |
| 2003 | 462 ± 39 | 35.336 ± 0.001 | 6.059 ± 0.004 | 76.7 ± 0.2 | 18.7 ± 1.0 | 25.1 ± 0.9 | | |
| 2009 | 411 ± 22 | 35.333 ± 0.001 | 5.953 ± 0.004 | 73.6 ± 0.2 | 20.7 ± 1.0 | 27.7 ± 0.9 | | |
| LSW | | | | | | | 0.47 ± 0.08 | 0.59 ± 0.05 |
| 1993 | 437 ± 54 | 35.112 ± 0.001 | 4.247 ± 0.005 | 71.2 ± 0.2 | 10.5 ± 1.2 | 13.6 ± 1.2 | | |
| 1998 | 339 ± 47 | 35.061 ± 0.001 | 4.004 ± 0.006 | 64.0 ± 0.3 | 12.1 ± 1.2 | 16.5 ± 1.3 | | |
| 2003 | 473 ± 41 | 35.100 ± 0.002 | 4.218 ± 0.007 | 67.5 ± 0.4 | 16.2 ± 1.8 | 20.4 ± 1.5 | | |
| 2009 | 406 ± 33 | 35.074 ± 0.001 | 4.088 ± 0.005 | 61.8 ± 0.2 | 17.5 ± 1.2 | 22.8 ± 1.2 | | |
| deep mixed | | | | | | | 0.16 ± 0.06 | 0.16 ± 0.02 |
| 1993 | 673 ± 78 | 34.990 ± 0.001 | 3.104 ± 0.004 | 69.9 ± 0.2 | 7.3 ± 1.0 | 8.2 ± 1.0 | | |
| 1998 | 883 ± 63 | 34.993 ± 0.001 | 3.161 ± 0.004 | 71.1 ± 0.2 | 7.3 ± 0.9 | 9.0 ± 0.8 | | |
| 2003 | 833 ± 78 | 34.982 ± 0.001 | 3.038 ± 0.004 | 70.2 ± 0.2 | 9.4 ± 1.0 | 10.1 ± 1.1 | | |
| 2009 | 880 ± 55 | 34.979 ± 0.001 | 2.990 ± 0.004 | 71.4 ± 0.2 | 9.4 ± 0.9 | 10.6 ± 0.9 | | |
| NADW | | | | | | | 0.01 ± 0.07 | 0.02 ± 0.01 |
| 1993 | 1 710 ± 151 | 34.916 ± 0.001 | 2.216 ± 0.003 | 84.7 ± 0.2 | 4.8 ± 0.8 | 1.4 ± 0.8 | | |
| 1998 | 1 584 ± 142 | 34.911 ± 0.001 | 2.184 ± 0.003 | 85.0 ± 0.2 | 3.6 ± 0.8 | 1.6 ± 0.8 | | |
| 2003 | 1 523 ± 200 | 34.908 ± 0.001 | 2.160 ± 0.003 | 84.8 ± 0.1 | 5.1 ± 0.8 | 1.4 ± 0.9 | | |
| 2009 | 1 572 ± 85 | 34.917 ± 0.001 | 2.219 ± 0.003 | 84.9 ± 0.1 | 4.5 ± 0.7 | 1.7 ± 0.7 | | |
| **$C_{ant}$ storage (molC m$^{-2}$)** | | | | | | | | |
| 1993 | | | | | 66.9 ± 4.1 | 67.9 ± 4.0 | | |
| 1998 | | | | | 68.3 ± 4.1 | 73.8 ± 4.2 | | |
| 2003 | | | | | 78.9 ± 4.2 | 85.0 ± 4.1 | | |
| 2009 | | | | | 88.1 ± 3.8 | 93.7 ± 3.7 | | |
| **$C_{ant}$ storage rate (molC m$^{-2}$ y$^{-1}$)** | | | | | | | 1.41 ± 0.25 | 1.67 ± 0.13 |

593

**Figure captions**

Figure 1. Iberian basin region and location of the cruises included in the study: OACES 1993, CHAOS 1998, OACES 2003 and CAIBOX 2009. In CAIBOX 2009 only the 20ºW section (empty circles in bold) was taken for the study.

Figure 2. Correlation between calculated and measured $C_T$. Units in $\mu mol \cdot kg^{-1}$. The linear equation of the fit is: $[C_T \text{ (calc)}-2000] = (0.9997 \pm 0.0109) \cdot [C_T \text{ (meas)}-2004.6 \pm 1.9]$ with a $R^2=0.994$ (n=50).

Figure 3. Vertical profiles of $C_{ant}$ estimated from $\varphi C_T^o$ and TrOCA methods in the Iberian basin.

Figure 4. Correlation between estimated data calculated by TrOCA and $\varphi C_T^o$ method for each cruise. Fit equations and determination coefficients for each of them are also given.

Figure 5. 20ºW vertical distributions of: a) AOU ($\mu mol \cdot kg^{-1}$, b) $A_T$ ($\mu mol \cdot kg^{-1}$) and c) $C_T$ ($\mu mol \cdot kg^{-1}$).

Figure 6. T-S diagram with the locations of the principal water masses of the region (black dots). Circles correspond to CAIBOX 2009 cruise data, triangles correspond to OACES 2003 data, and crosses and squares correspond to CHAOS 1998 and OACES 1993 data, respectively. The six layers in which the water column was divided are also shown: a) upper layers: NACW, MW and MW-LSW layers and b) deep layers: LSW, Deep Mixed and NADW layers. The isopycnals that limit each one of the layers are also represented (dashed lines).

Figure 7. Time evolution of $C_{ant}$ ($\mu mol \cdot kg^{-1}$) estimated from $\varphi C_T^o$ (continuous lines) and TrOCA (dashed lines) approaches in each layer (full symbols: sums, diamonds, crosses, squares, circles and triangles) and of $C_{ant}$ storages in $molC \cdot m^{-2}$ (empty circles). The $C_{ant}^{sat}$ (empty squares) is also shown in $\mu mol \cdot kg^{-1}$.

622 Figure 1

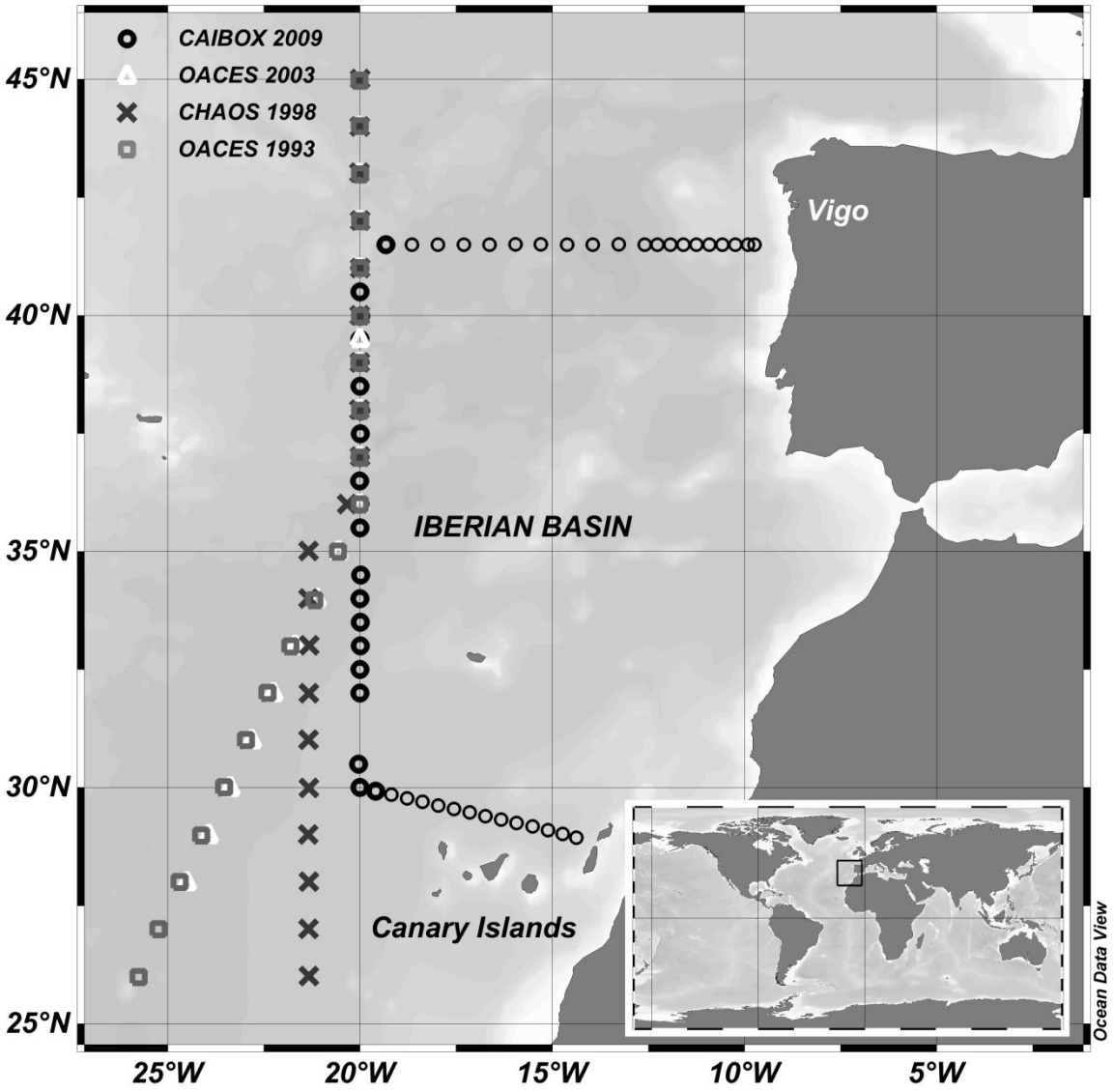


623

624

625

626 Figure 2

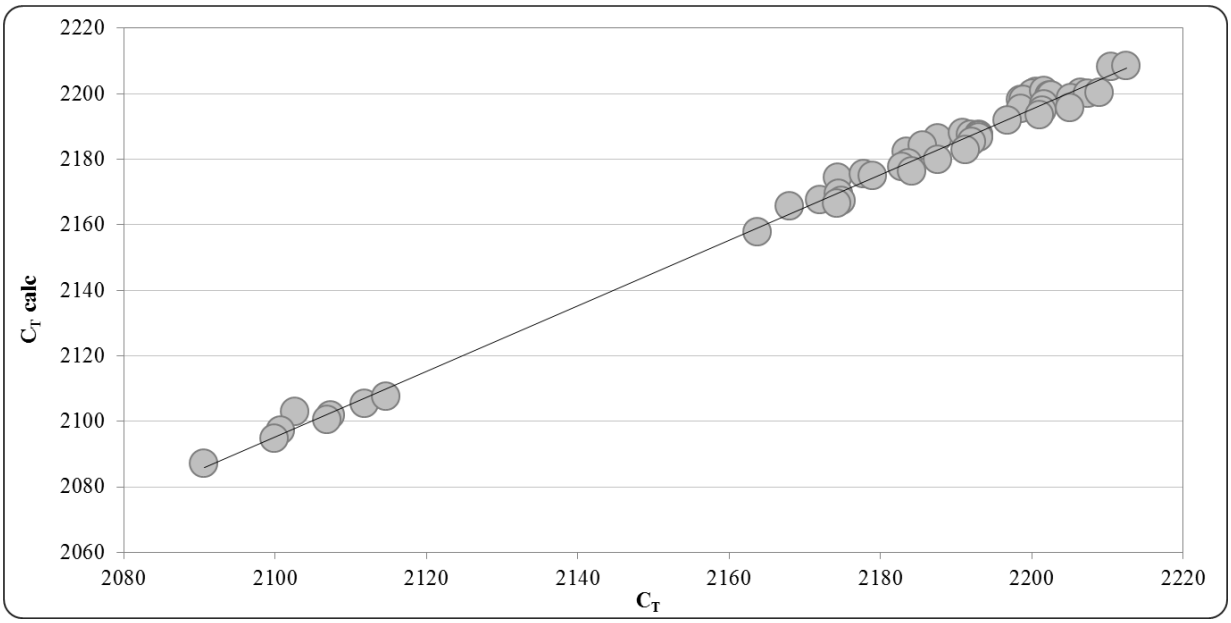


627

628

629

630

631 Figure 3

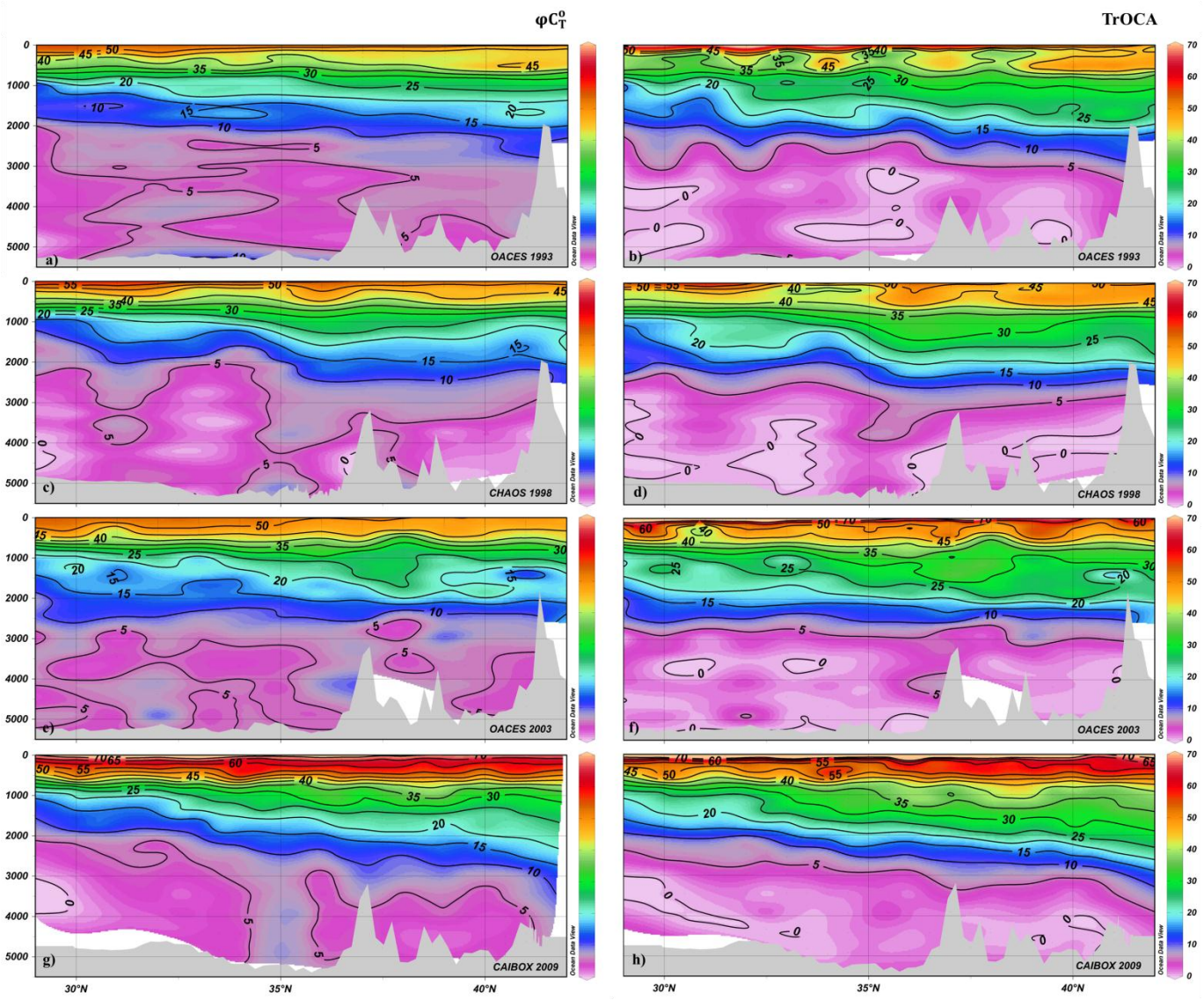


632

633

634 Figure 4

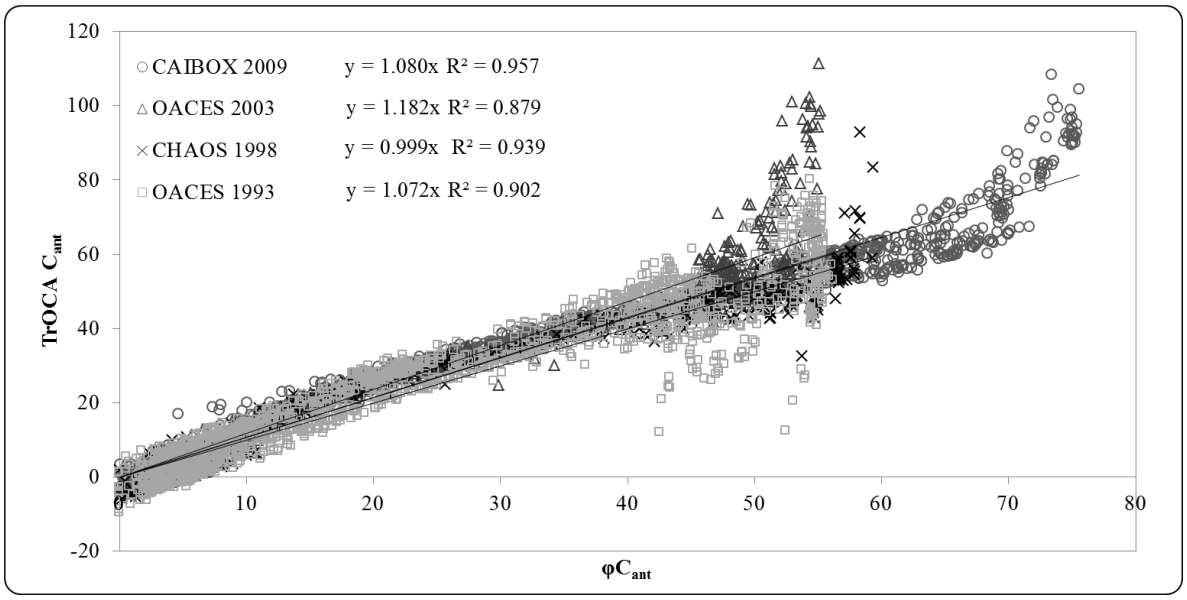


635

636

637 Figure 5

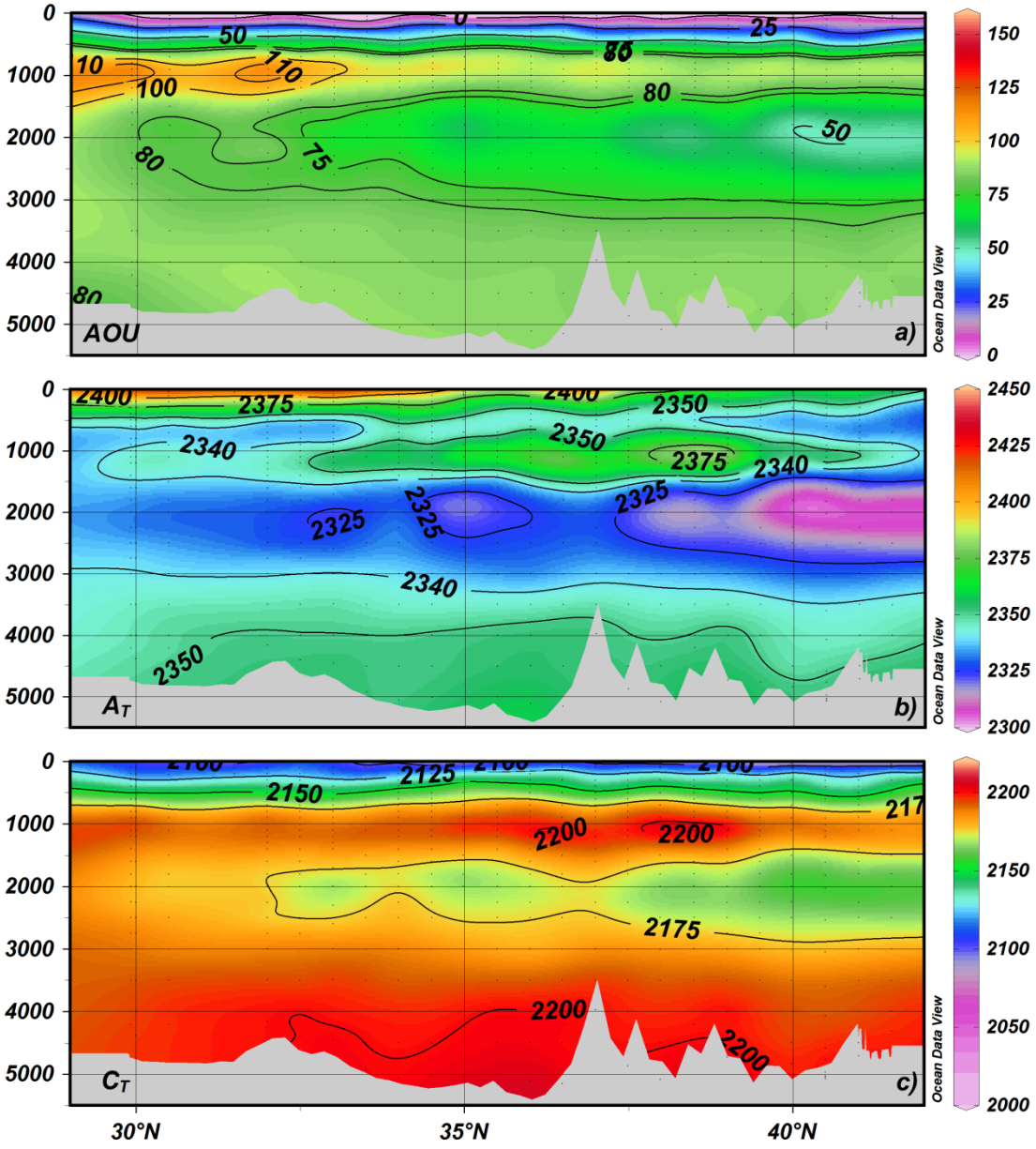


638

639

640

Figure 6

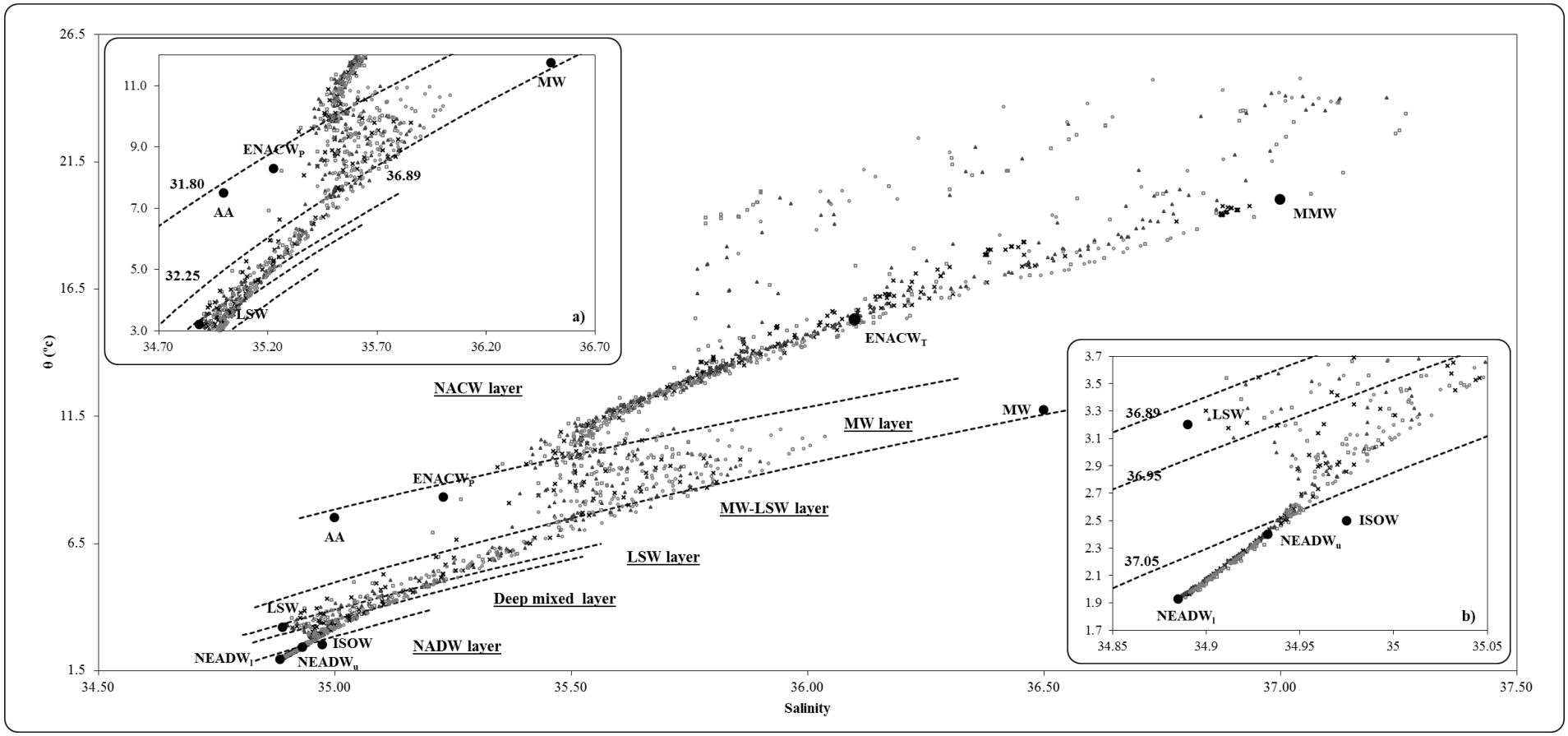
θ (°c)
Salinity
NACW layer
MW layer
MW-LSW layer
LSW layer
Deep mixed layer
NADW layer
ENACW$_T$
ENACW$_P$
MW
MMW
AA
LSW
ISOW
NEADW$_l$
NEADW$_u$
31.80
32.25
36.89
36.89
36.95
37.05
a)
b)

646 Figure 7

647

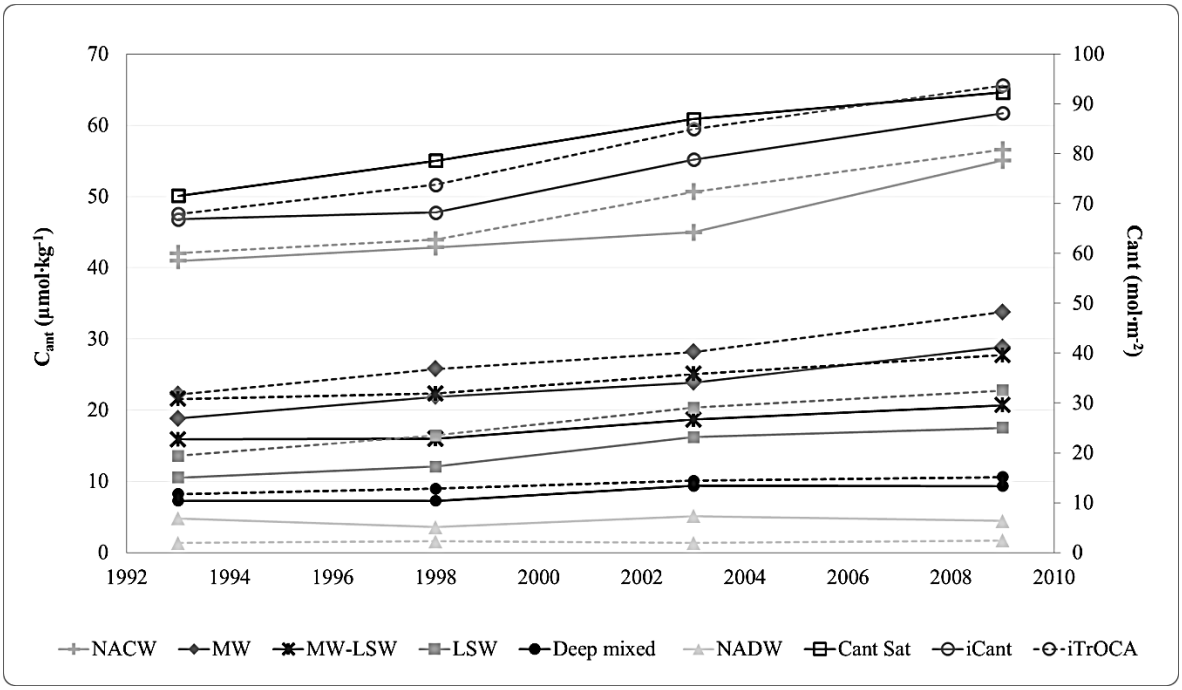


648

649